EFFECT OF OBSTACLES ON TURBULENT FLOWS IN A RECTANGULAR CHANNEL FROM THEIR FRONT SIDES

by

Zakaria SARI HASSOUN[a], Khaled ALIANE[a], Yun-Hui ZHAO[b*], Hijaz AHMAD[c,d], Younes MENNI[e], and Giulio LORENZINI[f]

[a] MECACOMP Laboratory, Department of Mechanical Engineering, Faculty of Technology, Abou Bekr Belkaid University of Tlemcen, Chetouane, Tlemcen, Algeria
[b] School of Mathematics and Information Science, Henan Polytechnic University, Jiaozuo, China
[c] Operational Research Center in Healthcare, Near East University, Nicosia/Mersin, Turkey
[d] Section of Mathematics, International Telematic University Uninettuno, Roma, Italy
[e] Department of Technology, University Center Salhi Ahmed Naama, Naama, Algeria
[f] Department of Industrial Engineering, University of Parma, Parma, Italy

Original scientific paper
https://doi.org/10.2298/TSCI23S1333S

In this piece, the impact of an obstacle's upstream edge inclination in a rectangular channel is investigated. The main purpose of this study is to give a better understanding of this associated phenomenon by reflecting more accurately the different cooling techniques and to get as close as possible to real conditions of use. This study is based on the laws of conservation of mass, momentum, and energy, the equations are given in the case of the 2-D flow of an incompressible Newtonian fluid, depending on the variables primitives given below. During the study, we used the FLUENT computer code, as well as its GAMBIT mesh generator several times, which allowed us to become more familiar with numerical simulation. The purpose of our numerical research is to clarify physical phenomena that are described by theory without using more expensive experimentation.

Key words*: turbulent flows, staggered obstacles, upstream edges of obstacles, streamlines, dynamic-pressure, velocity, numerical study*

Introduction

Heat transfer ducts are essential for many different industries and applications, so it was vital to investigate ways to enhance their efficiency. As is common knowledge, the baffling approach has been used by numerous researchers, particularly in the fields of solar energy and mechanics. Recent research has been taken into account for various impediments, under various flow conditions, and with various physical features [1-5]. Using CFD, Keramat and Izadpanah [6] examined the thermal hydraulic performance of a convergent and divergent heat exchanger with inclined-type fins. According to the results based on the friction and Colburn factors, the converging-diverging configurations report a greater rate in the heat transfer between 50.67% and 60.86% with a penalty for pressure-drop between 73.45% and 86.90% when compared to cylindrical-type heat-exchangers. In addition, the heat transfer is improved by the inclined-type fins by up to 21.65% as compared to the vertical-type fins. Finally, taking into account the area goodness factor, the ideal heat-exchanger lay-out is

* Corresponding author, e-mail: zhaoyunhui2019@163.com

presented. To improve its flow-field performance, a tubular-type swirl-flow solar-heater at air with a novel semi-cylindrical-type absorber-plate is used in El-Said *et al*. [7] research. Tests on the proposed heater are conducted using both radial and longitudinal fins. There are three sets of fins that are tested: 3-5. Under typical rates of air-flow of 0.01-0.50 kg/s, and Reynolds numbers ranging from 7078-35190, data from the proposed heater are compared with those from the plain channel conventional heater with no fins. The study's findings showed that, when compared to a simple heater or a heater with longitudinal-section fins, radial fins improve heater performance metrics. The study conducted by Saravanakumar *et al*. [8] focused on the parameter optimization of a solar-air-heater with arc-shaped ribs that were combined with baffles and fins. The effect of geometrical and operational parameters on the exergy efficiency of the considered heater has been investigated using theoretical analysis based on exergy loss. It is discovered that the suggested heater's maximum exergy efficiency at ideal conditions is 5.2%. It is clear from the plots that a baffle with a length of 0.2 m, a width of 0.015 m, and a rate of mass-flow of 0.012 kg/s will provide the most exergy. With models found in the literature, the simulation findings of the current model for the proposed heater have been validated and confirmed to be in good accord. Furthermore, Feng *et al*. [9] examined the trapezoidal baffle's synergistic impact on the fluid and heat transmission in the flow channel. The outcomes demonstrated that the trapezoidal-type baffle can enhance the field synergistic effect and enhance the overall heat transfer performance of the flow channel by encouraging fluid mixing and momentum exchange. The PEC value can be raised by 30%, and the Nusselt number and f of flow channels fitted by trapezoidal baffles were more than 1.7 and 3.5 times greater than those with no baffles. The impact of utilizing perforated turbulators on the thermohydraulic properties of a rectangular channel has been explored experimentally and numerically in the work reported by El Habet *et al*. [10]. The investigation's findings showed that all of the suggested turbulator lay-outs significantly increase heat transfer by roughly 410% when compared to a smooth channel. It is noted that the inline design exhibits greater friction loss than the staggered lay-out across the whole range of perforation ratios and under the identical operating conditions. Additionally, both baffle designs with reduced perforation ratio have greater thermal performance. Tian *et al*. [11] suggested a heat exchanger containing perforated barriers. The findings indicated that, at a flow rate of 0.1280 kg per second, introducing porous obstacles, *i.e*., baffles and fins, may promote heat transfer by 92.14%, decrease pressure loss by 64.70%, and reduce weight by 11.35%. Alnak [12] performed a computational analysis of the thermo-hydraulic performance, pressure loss, and heat intensification in triangular-shaped ducts with rectangular barriers. In their investigation, the 90° rectangle barrier in the case of a corrugated duct has a Nusselt value that is 52.8% greater than the 60° rectangle barrier with Re = 6000. Additionally, the pressure loss value for Re = 1000 is 65.97% smaller in the corrugated triangular-shaped duct fitted by a 60° rectangular barrier angle than it is in the duct with a 90° angle. Other important studies can be found in [13].

The numerical analysis of the turbulent air-flow in forced convection around the barriers will be of particular interest to us in this work. In this piece, the impact of an obstacle's upstream edge inclination in a rectangular channel is investigated. The goal is to manage the flow around the obstruction. The presentation of the mathematical formulation as well as the physical and numerical models that will be examined are both covered in the second section. The simulation results provided by FLUENT and their comments are shown in section three. A conclusion that summarizes the work done is also included in this paper.

Mathematical modelling

The study was conducted around a heat exchanger, its channel is horizontal rectangular, containing extended surfaces in the form of obstacles attached in a periodically staggered manner. A detailed geometric representation is shown in fig. 1.

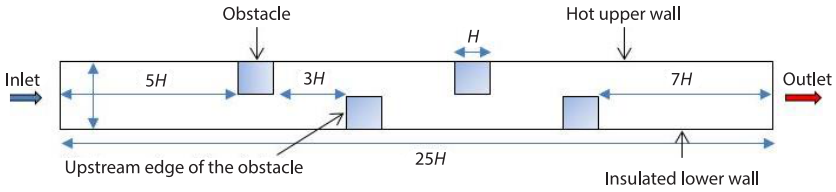

Figure 1. The heat exchanger model under study

In order to determine the ideal setting for enhanced fluid transport, we primarily concentrate on an essential geometric variable connected to barriers in this study, namely the effect of the inclination of their upstream edges. Three scenarios can occur depending on the angle of inclination, θ, of the obstacle's upstream edge:

– Square obstacles in the case where $\theta = 0$, see fig. 2(a).
– Trapezoidal obstacles in the case where $0 < \theta < 45°$, see fig. 2(b).
– Triangular obstacles in the case where $\theta = 45°$, see fig. 2(c).

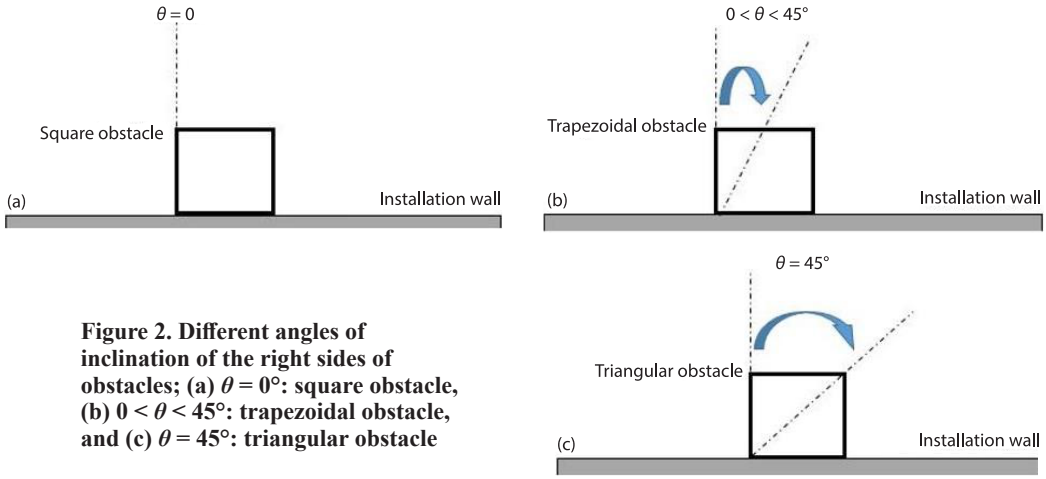

Figure 2. Different angles of inclination of the right sides of obstacles; (a) $\theta = 0°$: square obstacle, (b) $0 < \theta < 45°$: trapezoidal obstacle, and (c) $\theta = 45°$: triangular obstacle

The dimensions of specific geometry are displayed in tab. 1.

Table 1. Geometric dimensions of the current heat exchanger canal

Dimension	In terms of dimension H
Channel length	25H
Channel height	2H
Hydraulic channel diameter	2H
Obstacle width	1H
Obstacle height	1H
Separation distance from obstacles	3H
The distance between the channel entrance and the left side of the first obstacle	5H
The distance between the right side of the last obstacle and the exit from the conduit	7H

where $H = 0.01$ m. The following theories were taken into account to simulate air-flow in the physical model being examined:

– the air-flow is stationary,
– the air-flow is 2-D,
– the air-flow is turbulent,
– the air-flow is Newtonian,
– the air-flow is incompressible,
– the air fluid's thermophysical characteristics are regarded as constant,
– the aluminum solid's thermophysical characteristics are regarded as constant,
– at the channel inlet, the air fluid has an uniform velocity profile, U_{in}, [13], and
– the standard k-ε turbulence model [14] is considered to model the air-flow.

The conservation equation of a scalar variable, ϕ, can be written in 2-D [15]:

$$\frac{\partial}{\partial x}(\rho u\phi)+\frac{\partial}{\partial y}(\rho v\phi)=\frac{\partial}{\partial x}\left[\Gamma_\phi\frac{\partial\phi}{\partial x}\right]+\frac{\partial}{\partial y}\left[\Gamma_\phi\frac{\partial\phi}{\partial y}\right]+S_\phi \tag{1}$$

where ϕ is a variable that serves to represent quantities such as: u and v the velocity components, k the turbulent kinetic energy, and ε the rate of turbulent energy dissipation.

However, the coefficient of diffusion Γ_ϕ and the source term S_ϕ have specific values for the different conservation equations for the case of the standard k-ε turbulence model [15] contains additional information.

The GAMBIT created the computational domain. The mesh was improved close to the channel walls and obstructions in order to manage flow changes near the wall. Mesh sizes for conduit length and depth ranged from 50-300 and 10-100, respectively. With the (170 × 50) mesh, the results demonstrate a negligibly small variance in velocity values (less than 0.25%). All computations made use of this mesh size.

The FLUENT was used in this investigation. Utilizing the second-order upwind [16] and QUICK [17] numerical schemes, respectively, the terms of pression and convection were discretized. The SIMPLE [16] algorithm was used to carry out the coupling velocity-pression. As a convergence criterion, the residual goal of 10-6 was accepted. More information on the validity of the numerical model can be found in [18].

Findings and analysis

Figure 3 represents the evolution of the streamlines for the different obstacle situations ($\theta = 0°$: square obstacle, see fig. 3(a); $0 < \theta < 45°$: trapezoidal obstacle, see fig. 3(b), and $\theta = 45°$: triangular obstacle, see fig. 3(c)). We observe that the streamlines change between the three forms 3(a)-3(c) depending on the obstacle. In fig. 3(a) (square case), the streamlines are less contoured as they pass over the obstacle and create turbulence that disrupts the flow. In fig. 3(b) (trapezoidal case), the streamlines are straightened as they pass over the obstacle, which varies the field direction of the streamlines. In fig. 3(c) (triangular case), the streamlines are glued to the obstacle, which gives us a formidable field of streamlines.

The flows in the air streams for the three types of obstacles generate complex phenomena such as re-circulation zones and regions of turbulence upstream and downstream of the obstacles, as illustrated by fig. 3. It should be noted for the three air streams that the presence of the obstacles causes the flow to separate into several different zones above, downstream and upstream of the obstacles. The flow thus forms re-circulation zones near the lower obstacles (Zone A), which increases the intensity of the turbulence upstream of the upper obstacles (Zone B). In addition the separation of the flow of fluid caused by the obstacles, there are dead

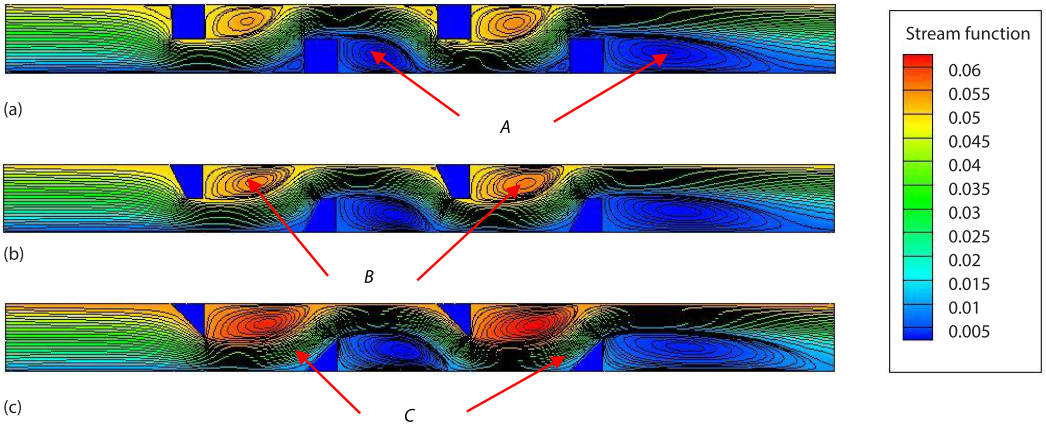

Figure 3. Contour plots of streamlines for different angles of attack of obstacles; (a) $\theta = 0°$: square obstacle, (b) $0 < \theta < 45°$: trapezoidal obstacle, and (c) $\theta = 45°$: triangular obstacle, Re = 2.500

zones upstream of the lower obstacles (Zone C), we notice that the dead zone for the case of trapezoidal shaped obstacles is less important compared to the square obstacles, and the dead zone is almost zero for the model which contains triangular obstacles. The turbulent zone (Zone B) for the model containing triangular obstacles is very large compared to other models which contain square and trapezoidal obstacles.

The general dynamic pressure configuration for the three types studied is similar, as shown in fig. 4. At the entrance, the dynamic pressure is uniform just below the first upper obstacle zone, the dynamic pressure takes almost zero values upstream of the upper and lower obstacles. The sharp upstream edge presents a point of separation in the Zones (A, B, C, and D) where the dynamic pressure is very high. However, the flow detaches from the wall of the obstacle, which causes a depression downstream of these obstacles.

In fig. 4(a), the dynamic pressure is almost zero soft the attack bornes, because the bad circulation in this point. In fig. 4(b), the dynamic pressure must be moved away along the profile, resulting in an average flow of kinetic energy. In fig. 4(c), the pressure has a significant value because the profile is perfect, which gave us a great movement.

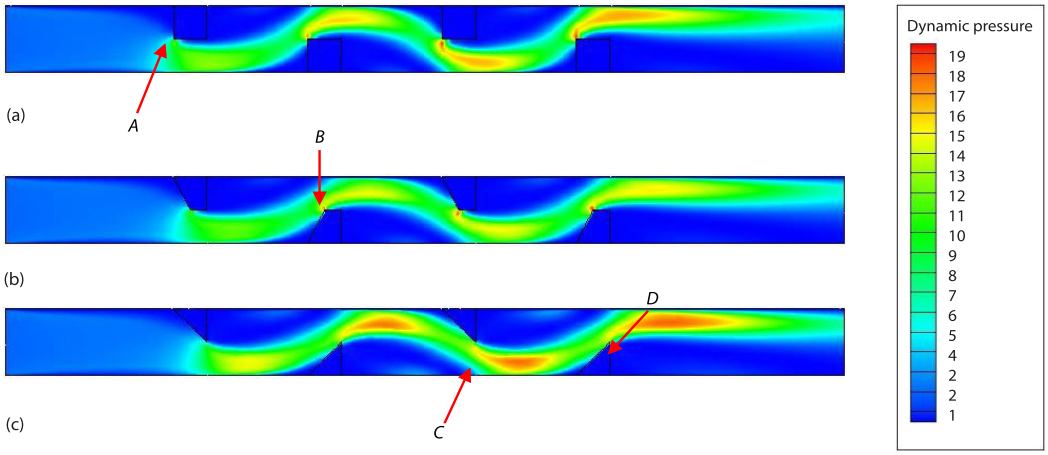

Figure 4. Contour plots of dynamic-pressure fields for different θ cases; (a) $\theta = 0°$: square obstacle, (b) $0 < \theta < 45°$: trapezoidal obstacle, and (c) $\theta = 45°$: triangular obstacle, Re = 2500

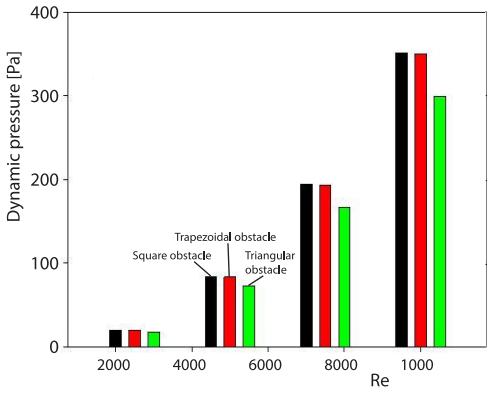

Figure 5. Effect of the inclination of the upstream edge of the obstacle on the dynamic pressure (maximum) for various values of the Reynolds number

Figure 5 represents the dynamic pressure variation as a function of the Reynolds number (Re = 2500, 5000, 7500, and 10,000) for the three forms of obstacle ($0 \leq \theta \leq 45°$). Note that each time the higher the Reynolds number, the greater the pressure. As we see that the value of the pressure in both cases, the square obstacle and the trapezoidal obstacle are very close. In addition, the pressure value in the case of the triangular is rather low, unlike the two previous cases. In fig. 5(b), the dynamic pressure must be moved away along the profile, resulting in an average flow of kinetic energy. In fig. 5(c), the pressure has a significant value because the profile is perfect, which gave us a great movement.

Figure 6 shows that the vortex is always generated upstream of the rectangular obstacle. On the other hand, the flow always remains stuck to the wall of the obstacle at the level of the triangular and trapezoidal obstacle and continues to follow the wall. There are therefore, two important points in the flow. The figures clearly show that the influence of the ridge downstream of the obstacle is not limited to the re-circulation zone but it modifies the behavior of the fluid even upstream of this ridge and clearly shows that the flow adheres to the upper wall of the triangular obstacle. This allows us to say that the existence of the inclination at the level of the edge upstream of the obstacle does not only control the zone of the triangle, but its effect is extended to the surroundings of this obstacle.

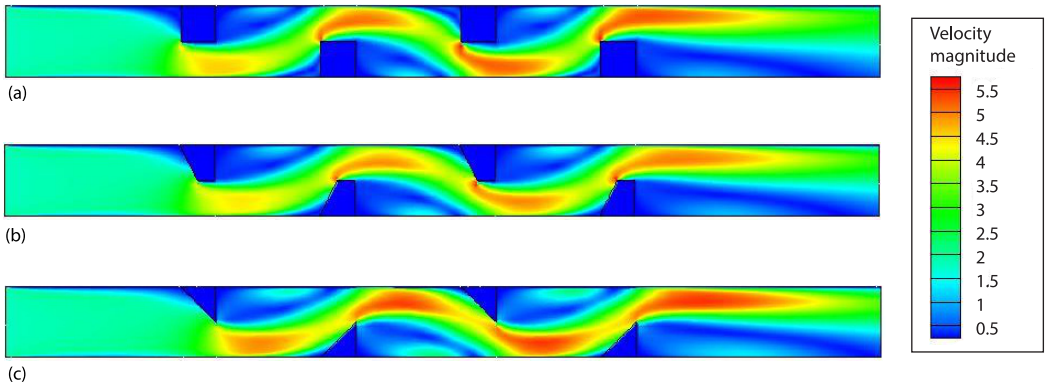

Figure 6. Contours of mean velocity fields for different angles of obstacle attack; (a) $\theta = 0°$: square obstacle, (b) $0 < \theta < 45°$: trapezoidal obstacle, and (c) $\theta = 45°$: triangular obstacle, Re = 2500

Several zones are distinguished in the three models studied and this according to the average intensity of the speed (low or high). The average speeds are low just upstream of the first obstacle for the three models studied. They are also weak downstream of square, trapezoidal and triangular obstacles. The average speeds are very high under the upper obstacles and the lower obstacles for the three models studied.

Figure 7 represents the distribution of the average speed as a function of the Reynolds number. It can be seen that the average speed increases following the increase in the Reynolds number only for the three models studied. If we make the comparison between the models for a Reynolds number, we notice that the values of the average speed for the model with square obstacles and the model with trapezoidal obstacles are almost equal, however they are 12% higher compared to the model with triangular obstacles.

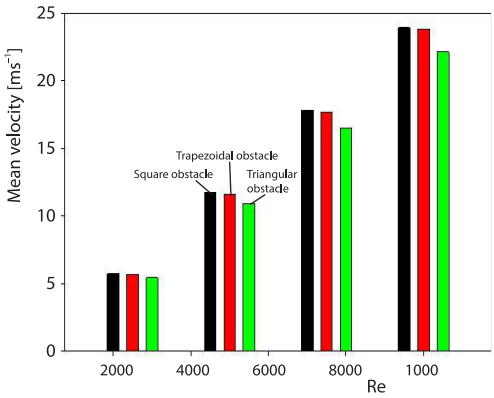

Figure 7. Effect of the inclination of the upstream edge of the obstacle on the average speed (maximum) for various values of the Reynolds number

Figure 8 represents the variation of the axial velocity as a function of the height of the channel at $x = 0.07$ m for different values of the Reynolds number and in all the cases considered. It is observed that, when the value of the channel height is between 0-0.015 m, the velocity is increased, where the velocity increases when the value of the Reynolds number increases. If we compare the axial velocity profiles for the three models with a Reynolds number, we observe that the velocities are almost similar for the models with square and trapezoidal obstacles, on the other hand the velocities take significant values for the model with obstacles triangular. According to the value of the height 0.015, we notice that the velocities take the opposite direction of the flow and the values of the velocities of the model with triangular obstacles are the greatest compared to the other models (Zone A).

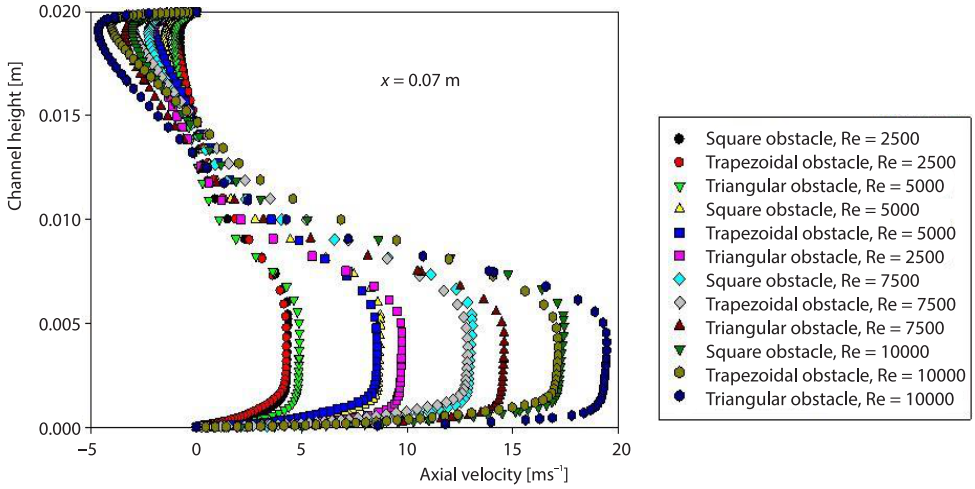

Figure 8. Profiles of the axial velocity, u, downstream of the first obstacle at $x = 0.07$ m for different angles of attack of obstacles and various values of the Reynolds number (*for color image see journal web site*)

Conclusion

The following are some of the main conclusions are as follows.

- The streamlines in the first model of the square situation are less contoured as they cross the obstacle, which causes turbulence to disturb the flow.
- The streamlines are straightened when they cross the obstruction in the second model of the trapezoidal problem, changing the streamlines' field direction.
- In the third triangular scenario model, the streamlines are adhered to the obstruction, creating a powerful field of streamlines.
- Complex phenomena, such as re-circulation zones and regions of turbulence upstream and downstream of the barriers, are produced by the fluxes in the air streams for the three different types of obstacles.
- In comparison square obstacles, the dead zone for trapezoidal obstacles is reported to be less important, and for the model with triangle obstacles, the dead zone is almost non-existent.
- In contrast to other models that have square and trapezoidal barriers, the model with triangle obstacles has a fairly extensive re-circulation zone.
- It is noted that the square and trapezoidal obstacles have relatively similar pressure values in both situations. In contrast to the preceding two situations, the pressure value in the triangular case is also quite modest.
- The values of the average speed for the model with square and trapezoidal obstacles are almost equal, however they are 12% higher compared to the model with triangular obstacles.
- Due of the constant section and changing flow, the varied Reynolds numbers result in a variation in speed.

References

[1] Abdi, G., *et al.*, The 3-D Evaluation of a Thermal and Hydraulic Winged Solar Collector, *Instrumentation, Mesures, Métrologies*, *21* (2022), 2, pp. 35-41
[2] Boursas, A., *et al.*, Enhanced heat Transfer by Oil/Multi-Walled Carbon NanoTubes Nanofluid, *Annales de Chimie-Science des Matériaux*, *45* (2021), 2, pp. 93-103
[3] Menni, Y., *et al*., Analysis of Thermo-hydraulic Performance of a Solar Air Heater Tube with Modern Obstacles, *Archives of Thermodynamics*, *41* (2020), 3, pp. 33-56
[4] Chamkha, A. J., Menni, Y., Hydrogen Flow over a Detached V-shaped Rib in a Rectangular Channel, *Mathematical Modelling of Engineering Problems*, *7* (2020), 2, pp. 178-186
[5] Jiang, Y., *et al*., Effect of Area Ratio and Reynolds Number on the Distribution of Discharge in Dividing Manifold, *International Journal of Low-Carbon Technologies*, *17* (2022), May, pp. 1271-1279
[6] Keramat, F., Izadpanah, A. A., Thermo-Hydraulic Performance Analysis of Converging-Diverging Heat Exchanger With Inclined Fins Using Computational Fluid Dynamics, *Journal of the Taiwan Institute of Chemical Engineers*, *132* (2022), 104119
[7] El-Said, E. M., *et al*., Tubular Solar Air Heater Using Finned Semi-Cylindrical Absorber Plate With Swirl Flow: Experimental Investigation, *Solar Energy*, *236* (2022), Apr., pp. 879-897
[8] Saravanakumar, P. T., *et al*., Exergetic Investigation and Optimization of Arc Shaped Rib Roughened Solar Air Heater Integrated With Fins And Baffles, *Applied Thermal Engineering*, *175* (2020), 115316
[9] Feng, C. N., *et al*., Friction Factor and Heat Transfer Evaluation of Cross-Corrugated Triangular Flow Channels With Trapezoidal Baffles, *Energy and Buildings*, *257* (2022), 111816
[10] El Habet, M. A., *et al.*, Thermal/Hydraulic Characteristics of a Rectangular Channel With Inline/Staggered Perforated Baffles, *International Communications in Heat and Mass Transfer*, *128* (2021), 105591
[11] Tian, H., *et al*., Assessment and Optimization of Exhaust Gas Heat Exchanger With Porous Baffles and Porous Fins, *Applied Thermal Engineering*, *178* (2020), 115446
[12] Alnak, D. E., Thermohydraulic Performance Study of Different Square Baffle Angles in Cross-Corrugated Channel, *Journal of Energy Storage*, *28* (2020), 101295
[13] Demartini, L. C., *et al*., Numeric and Experimental Analysis of the Turbulent Flow through a Channel With Baffle Plates, *Journal of the Brazilian Society of Mechanical Sciences and Engineering*, *26* (2004), 2, pp. 153-159

[14] Launder, B. E., Spalding, D. B., The Numerical Computation of Turbulent Flow, *Computer Methods in Applied Mechanics and Engineering*, *3* (1974), 2, pp. 269-289
[15] Yang, Y. T., Hwang, C. Z., Calculation of Turbulent Flow and Heat Transfer in a Porous-Baffled Channel, *International Journal of Heat and Mass Transfer*, *46* (2003), 5, pp. 771-780
[16] Patankar, S. V., *Numerical Heat Transfer and Fluid-Flow*, McGraw-Hill, New York, USA, 1980
[17] Leonard, B. P., Mokhtari, S., Ultra-Sharp Non-Oscillatory Convection Schemes for High-Speed Steady Multidimensional Flow, NASA TM 1-2568, NASA Lewis Research Center, Cleveland, O., USA, 1990
[18] Menni, S., Belabbaci, F., Study of the Dynamic Structure of Turbulent Flow around an Obstacle: Effect of Thermal Stratification, Etude des écoulements turbulents autours d'un obstacle: effet de la rugosité couplé à l'inclinaison (in French), M. Sc. thesis, Université Aboubakr Belkaïd-Tlemcen, 2022

Paper submitted: April 19, 2022
Paper revised: May 4, 2022
Paper accepted: June 17, 2022